Supporting Information for Mercury's low-degree geoid and topography controlled by insolation-driven elastic deformation

N. Tosi[1,2], O. Čadek[3], M. Běhounková[3], M. Káňová[3], A.-C. Plesa[2], M. Grott[2], D. Breuer[2], S. Padovan[2] and M. Wieczorek[4]

Corresponding author: N. Tosi, Department of Astronomy and Astrophysics, Technische Universität Berlin, Hardenberg Strasse 36, Berlin, Germany (nicola.tosi@tu-berlin.de)

[1]Department of Astronomy and Astrophysics, Technische Universität Berlin, Germany

[2]Department of Planetary Physics, German Aerospace Center (DLR), Berlin, Germany

[3]Department of Geophysics, Charles University, Prague, Czech Republic

[4]Institut de Physique du Globe de Paris, Sorbonne Paris Cité, Université Paris Diderot, Paris, France

Contents of this file

Introduction

In Section S1 of this supporting information we briefly describe the model used to obtain the surface temperature distribution plotted in Figure 1a and report in Table S1 the accompanying spherical harmonic expansion. In Section S2, we describe the elastic model and the equations we solved to calculate the mechanical and gravitational response of the mantle to internal loading due to mantle convection and insolation-driven thermal heterogeneities. The parameters used in this model are contained in Table S3. Tables S2 and S4 contain the parameters of the mantle convection model and those used to calculate the elastic thickness on the base of the strength-envelope formalism. Finally, Figure S1 shows two projections of the temperature field during the convective and the conductive phases of the evolution, while Figure S2 shows the effects of the coefficient of thermal expansion on the prediction of geoid and topography.

1. Surface temperature model

The temperature distribution shown in Figure 1a was obtained by reproducing model TWO of *Vasavada et al.* [1999]. This is a two-layer model consisting of a highly insulating, 2-cm-thick top layer overlying a more conductive and dense 78-cm-thick lower layer. We also tested model BOT, which differs from model TWO in that it consists of a single layer

with the properties of the bottom layer of model TWO and obtained best estimates of the elastic thickness differing only by few km. With these models, one can calculate the thermal response of shallow surface and subsurface layers to solar and infrared radiation in dependence of their material properties (solar albedo, infrared emissivity, density, thermal conductivity, and heat capacity). The temperature distribution that we employed in our simulations (shown in Figure 1a) actually corresponds to the subsurface temperature (at the bottom of the domain at a depth of 80 cm) where temperature changes along the orbit due to the skin effect are negligible. For a detailed description of this model, we refer the reader to *Vasavada et al.* [1999]. Here we limit ourselves to report in Table S1 the spherical harmonic expansion up to degree and order 4 of the resulting distribution of the near-surface temperature T^{surf} for two different normalizations of the spherical harmonic functions: complex orthonormalized (CSH) and real, 4π-normalized (RSH). The expansion was simply calculated by numerical integration of the temperature distribution obtained on a regular grid with 1-degree spacing both in latitude and in longitude. Note that because of the symmetry of this distribution with respect to both the equator and the 0° meridian, spherical harmonic coefficients of odd degree and/or order are zero, as are the imaginary part of the complex coefficients for the CSH-normalization and the sine terms for the RSH normalization.

2. Equations for the elastic model

The outer shell of Mercury, which consists of a crust of density ρ_{c} and thickness D_{c}, and mantle of density ρ_{m}, is divided into two parts: an elastic shell (lithosphere) of thickness D_{e} and the underlying mantle where shear stresses are assumed to be negligible (see Figure

2). As the viscous stresses due to mantle convection are small, the interface between mantle and liquid core is treated as an equipotential surface and its shape, $t_{\rm CMB}$, is fully determined by variations of the gravitational potential δV at the core-mantle boundary radius $R_{\rm CMB}$. Using Bruns' formula, we have:

$$t_{\rm CMB}(\vartheta,\varphi) = \frac{\delta V(R_{\rm CMB},\vartheta,\varphi)}{g(R_{\rm CMB})}\,, \tag{S1}$$

where ϑ and φ are the co-latitude and longitude, respectively.

The surface topography H results from the deformation of the elastic shell induced by temperature anomalies due to insolation that propagate from the surface to the CMB and, if present, due to mantle convection. The deformation of the elastic shell is a superposition of three contributions: 1) the deformation induced by buoyancy forces of thermal origin acting in the shell; 2) volumetric deformation within the shell due to thermal expansion and resulting from compressibility effects (see equation (S5)); and 3) volumetric changes due to temperature in the mantle below the shell, which induce the radial dilatation

$$\Delta R_{\rm th}(\vartheta,\varphi) = \int_{R_{\rm CMB}}^{R_{\rm e}} \alpha\delta T(r,\vartheta,\varphi){\rm d}r\,, \tag{S2}$$

where δT denote temperature anomalies (also derived form the mantle convection model). A small part of this dilatation is accommodated by the deflection of the core-mantle boundary, so that the final change in radius is

$$\Delta R = \Delta R_{\rm th} + t_{\rm CMB}. \tag{S3}$$

We assume that the elastic shell is Hookean and its mechanical properties are characterized by two parameters, shear modulus μ and bulk modulus K, with different values in the

crust and mantle (see Table S3). To evaluate the deformation of the elastic shell, we solve the following set of conservation equations, namely linear momentum (S4) and mass (S5) supplemented by a constitutive equation (S6), for three unknown quantities, namely the displacement $\boldsymbol{u}$, the increment of pressure p and the deviatoric stress $\boldsymbol{\sigma}$ [*Golle et al.*, 2012]:

$$-\nabla p + \nabla \cdot \boldsymbol{\sigma} + \alpha \rho \delta T g_0 \boldsymbol{e}_r + \rho \nabla \delta V = 0\,, \tag{S4}$$

$$\nabla \cdot \boldsymbol{u} = -\frac{p}{K} + \alpha \delta T\,, \tag{S5}$$

$$\boldsymbol{\sigma} = \mu \left[\nabla \boldsymbol{u} + (\nabla \boldsymbol{u})^{\tau} - \frac{2}{3} (\nabla \cdot \boldsymbol{u}) \boldsymbol{I} \right]\,, \tag{S6}$$

with boundary conditions

$$(-p\boldsymbol{I} + \boldsymbol{\sigma}) \cdot \boldsymbol{e}_r = -\rho_c (\boldsymbol{u} \cdot \boldsymbol{e}_r + \Delta R) g_0 \boldsymbol{e}_r \;\text{ for } r = R_\mathrm{p}\,, \tag{S7}$$

$$[(-p\boldsymbol{I} + \boldsymbol{\sigma}) \cdot \boldsymbol{e}_r]^{+}_{-} = (\rho_c - \rho_\mathrm{m}) (\boldsymbol{u} \cdot \boldsymbol{e}_r + \Delta R) g_0 \boldsymbol{e}_r \;\text{ for } r = R_c\,, \tag{S8}$$

$$(-p\boldsymbol{I} + \boldsymbol{\sigma}) \cdot \boldsymbol{e}_r = -\rho_0 \delta V \boldsymbol{e}_r \;\text{ for } r = R_\mathrm{e}. \tag{S9}$$

Here, α is the thermal expansivity, ρ the mean density ($\rho = \rho_c$ in the crust and ρ_m in the mantle), $\boldsymbol{I}$ the identity tensor, g_0 the radially symmetric part of the gravitational acceleration, $\boldsymbol{e}_r$ the unit radial vector, $\bullet^{\tau}$ denotes transposition of a tensor, and $[\bullet]^{+}_{-}$ the jump across the crust-mantle interface. The above equations are solved using spectral decomposition in ϑ and φ and finite differences in radius.

The gravitational potential δV is evaluated using the Newton integral and expressed in terms of spherical harmonics as follows:

$$\delta V(r,\vartheta,\varphi) = \sum_{\ell m} \delta V_{\ell m}(r) Y_{\ell m}(\vartheta,\varphi) = \sum_{\ell m} \left[U_{\ell m}(r) + W_{\ell m}(r) + X_{\ell m}(r) + Z_{\ell m}(r)\right] Y_{\ell m}(\vartheta,\varphi)\,, \tag{S10}$$

where $Y_{\ell m}$ are orthonormalized complex spherical harmonic functions that include the Condon-Shortley phase factor of $(-1)^m$ [e.g. *Varshalovich et al.*, 1989]:

$$\int_\Omega Y_{\ell m}(\vartheta,\varphi) Y^*_{\ell' m'}(\vartheta,\varphi)\, d\Omega = \delta_{\ell\ell'}\delta_{mm'}. \tag{S11}$$

$U_{\ell m}$, $W_{\ell m}$, $X_{\ell m}$, and $Z_{\ell m}$ in Equation (S10) denote the gravitational potential of degree ℓ and order m induced by internal temperature anomalies, topography of the surface, of the crust-mantle interface and of the core-mantle boundary, respectively:

$$U_{\ell m}(r) = -\frac{4\pi G r \rho \alpha}{2\ell+1}\left[\int_{R_{\rm CMB}}^{r} \delta T_{\ell m}(r') \left(\frac{r'}{r}\right)^{\ell+2} {\rm d}r' + \int_{r}^{R_{\rm p}} \delta T_{\ell m}(r') \left(\frac{r}{r'}\right)^{\ell-1} {\rm d}r'\right], \tag{S12}$$

$$W_{\ell m}(r) = \frac{4\pi G r \rho_{\rm c}}{2\ell+1}\left[w_{\ell m}(R_{\rm p}) + \Delta R_{\ell m}\right]\left(\frac{r}{R_{\rm p}}\right)^{\ell-1}, \tag{S13}$$

$$X_{\ell m}(r) = \frac{4\pi G r \Delta\rho_{\rm mc}}{2\ell+1}\left[w_{\ell m}(R_{\rm c}) + \Delta R_{\ell m}\right]\left[\Theta(R_{\rm c}-r)\left(\frac{r}{R_{\rm c}}\right)^{\ell-1} + \Theta(r-R_{\rm c})\left(\frac{R_{\rm c}}{r}\right)^{\ell+2}\right], \tag{S14}$$

$$Z_{\ell m}(r) = \frac{4\pi G r \Delta\rho_{\rm CMB}}{2\ell+1}(t_{\rm CMB})_{\ell m}\left(\frac{R_{\rm CMB}}{r}\right)^{\ell+2}, \tag{S15}$$

where G is the gravitational constant, w denotes the radial component of the displacement vector, and Θ is the Heaviside function. Finally, the spherical harmonic coefficients of the topography and geoid of degree ℓ and order m are then given by

$$H_{\ell m} = w_{\ell m}(R_{\rm p}) + \Delta R_{\ell m} \tag{S16}$$

and

$$N_{\ell m} = \frac{\delta V_{\ell m}(R_{\rm p})}{g_0(R_{\rm p})}\,, \tag{S17}$$

respectively.

References

Golle, O., C. Dumoulin, G. Choblet, and O. Čadek (2012), Topography and geoid induced by a convecting mantle beneath an elastic lithosphere, *Geophys. J. Int.*, *189*(1), 55–72.

Grott, M., and D. Breuer (2008), The evolution of the Martian elastic lithosphere and implications for crustal and mantle rheology, *Icarus*, *193*(2), 503–515.

Tosi, N., M. Grott, A.-C. Plesa, and D. Breuer (2013), Thermochemical evolution of Mercury's interior, *J. Geophys. Res. Planets*, *118*(12), 2474–2487, doi:10.1002/jgre.20168.

Varshalovich, D., A. Moskalev, and V. Khersonskii (1989), *Quantum theory of angular momentum*, World Scientific Publ., Singapore.

Vasavada, A., D. Paige, and S. Wood (1999), Near-surface temperatures on Mercury and the Moon and the stability of polar ice deposits, *Icarus*, *141*(2), 179–193.

Table S1. Spherical harmonic coefficients of the surface temperature distribution obtained from model "TWO" of *Vasavada et al.* [1999] used to plot Figure 1a. The second column refers to the real part of the coefficients assuming orthonormalized complex spherical harmonics (CSH), while the third column refers to cosine coefficients assuming 4π-normalised real spherical harmonics (RSH), which do not include the Condon-Shortley phase factor and are obtained dividing the complex ones by $\sqrt{4\pi/(2-\delta_{m0})}$. Because of the symmetry of the distribution, coefficients of odd degree and/or order as well as the imaginary part of CSH-coefficients and the sine term of RSH-coefficients are negligible.

(ℓ, m)	$T^{\rm surf}_{\ell m}$ (CSH)	$T^{\rm surf}_{\ell m}$ (RSH)
(0,0)	1319.47	372.22
(2,0)	-124.08	-35.00
(2,2)	62.27	24.84
(4,0)	-41.10	-11.59
(4,2)	17.99	7.18
(4,4)	-17.21	-6.86

Table S2. List of the parameters used in the 3-D thermal evolution model (Section 2.1). A detailed description of this model can be found in *Tosi et al.* [2013].

Parameter	Value
Planet radius	2440 km
Core radius	2040 km
Surface gravity	3.7 m s^{-2}
Surface temperature	Variable (see Figure 1a)
Initial mantle temperature	1900 K
Initial core temperature	1900 K
Reference temperature	1600 K
Reference viscosity	10^{21} Pa s
Activation energy	300 kJ mol^{-1}
Mantle density	3400 kg m^{-3}
Core density	7000 kg m^{-3}
Thermal conductivity	3 W m^{-1} K^{-1}
Thermal expansivity	3×10^{-5} K^{-1}
Mantle heat capacity	1200 J kg^{-1} K^{-1}
Core heat capacity	850 J kg^{-1} K^{-1}
Crust thickness	30 km
Crust concentration of Th	155 ppb
Crust concentration of U	90 ppb
Crust concentration of K	1288 ppm
Crust enrichment factor	2.7

Table S3. List of the parameters used in the 3D elastic model (Section 2.1 and Section S2). Symbols correspond to those used in Figure 2.

Parameter (symbol)	Value
Planet radius (R_p)	2440 km
Core radius (R_CMB)	2040 km
Surface gravity (g_0)	3.7 m s^{-2}
Crust density (ρ_c)	2900, 3000, 3100 kg m^{-3}
Mantle density (ρ_m)	3400 kg m^{-3}
Core density (ρ_co)	7000 kg m^{-3}
Crust thickness (D_c)	20, 30, 40 km
Elastic thickness (D_e)	10 – 400 km
Thermal expansivity (α)	$2.5, 3, 3.5 \times 10^{-5}$ K^{-1}
Crust shear modulus (μ_c)	3.5×10^{10} Pa
Mantle shear modulus (μ_m)	7×10^{10} Pa
Crust bulk modulus (K_c)	$(5/3)\mu_\mathrm{c}$
Mantle bulk modulus (K_m)	$(5/3)\mu_\mathrm{m}$

Table S4. List of the parameters used to calculate the elastic thickness based on the strength-envelope formalism (Section 3 and Equation (3)). Rheological parameters (activation energy, pre-factor, and stress exponent) are appropriate of a dry diabase crust and a dry olivine mantle (see *Grott and Breuer* [2008] for details).

Parameter (symbol)	Value for the crust	Value for the mantle
Bounding stress (σ_y)	15 MPa	15 MPa
Activation energy (Q)	488 kJ mol^{-1}	540 kJ mol^{-1}
Pre-factor (B)	1.1×10^{-26} Pa^{-n} s^{-1}	2.4×10^{-16} Pa^{-n} s^{-1}
Stress exponent (n)	4.7	3.5
Strain rate ($\dot{\epsilon}$)	10^{-19}–10^{-17} s^{-1}	10^{-19}–10^{-17} s^{-1}

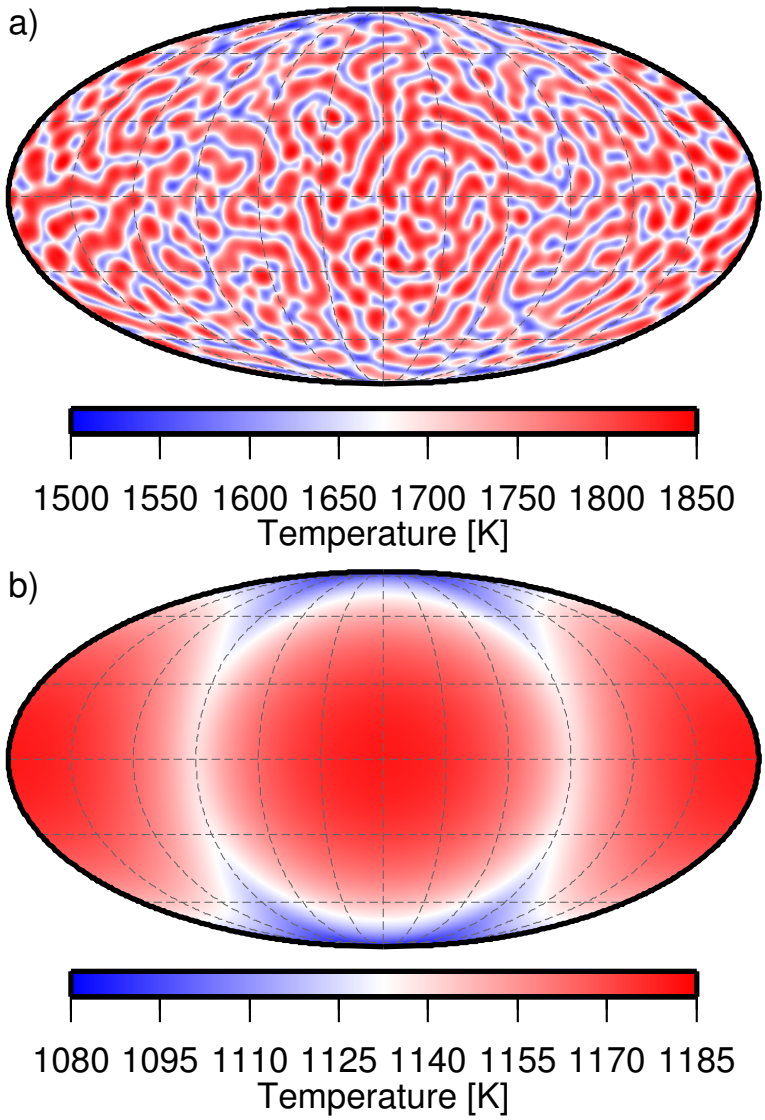

Figure S1. (a) Convective and (b) conductive temperature distribution at mid-mantle depth after 1 Gyr of evolution and at present-day, respectively. Note that even during the convective phase the effects of the surface temperature pattern are still recognizable in the cold downwellings that concentrate at the poles and along the ±90° meridians.

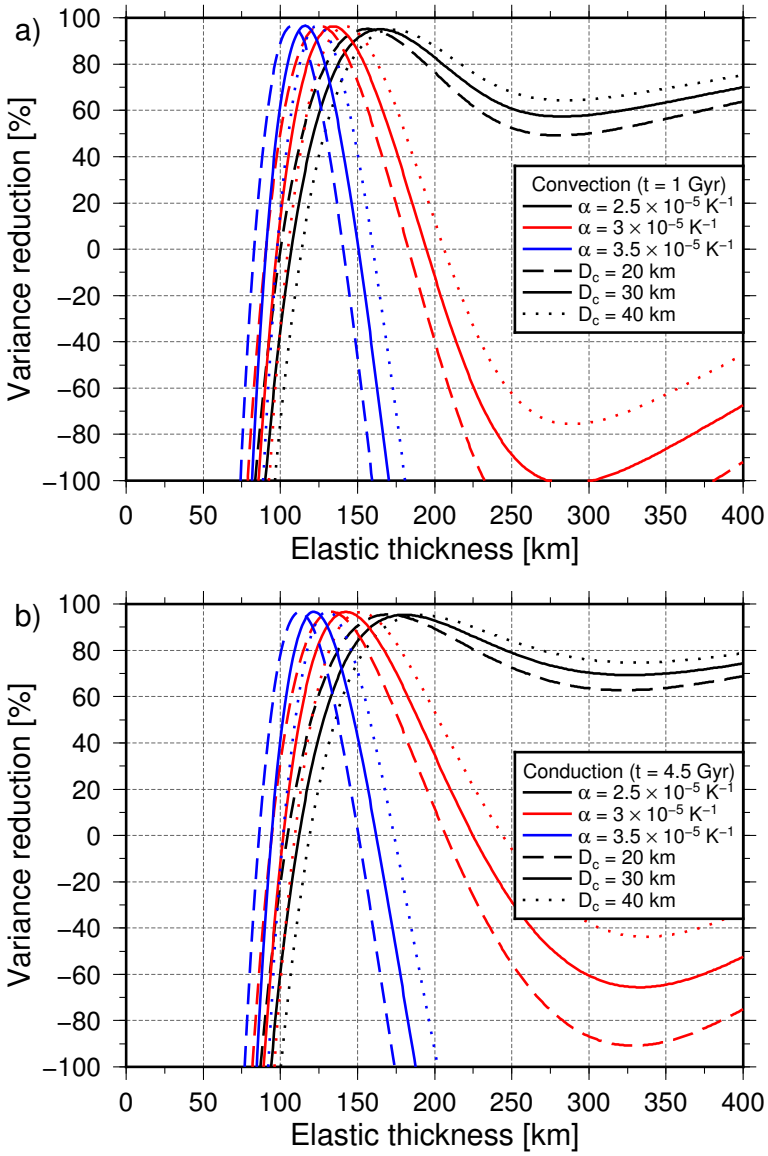

Figure S2. (a) Variance reduction $\mathcal{P}_{N,H}$ as a function of the elastic thickness for the convective solution after 1 Ga of evolution, different values of the coefficient of thermal expansion α and different depths D_c at which the crust-mantle density contrast is imposed. (b) As in panel a, but for the present-day conductive solution.